RESEARCH

The lowest singlet states of hexatriene revisited

Riccardo Guareschi[1] · Celestino Angeli[2]

Abstract

The two lowest excited singlet states of *trans*-hexatriene and *cis*-hexatriene are studied by multireference perturbation theory approaches (NEVPT2 and CASPT2) in their quasi-degenerate version (QD-NEVPT2 and MS-CASPT2). For these states, we report spectroscopic properties such as the vertical and adiabatic excitation energies, some features of the topology of the potential energy surfaces (PES), and the emission energies. The theoretical vertical excitation energies for the $2\,^1A_g^-$ and $1\,^1B_u^+$ states of *trans*-hexatriene are found to be almost degenerate, with a value, $\simeq 5.5$–5.6 eV, higher than that normally accepted in the literature, 5.2 eV and 5.1 eV, respectively. The $2\,^1A_1$ and $1\,^1B_2$ states of *cis*-hexatriene are also almost degenerate and are estimated to be at $\simeq 5.4$–5.5 and $\simeq 5.5$ eV, respectively, again higher than the accepted values. The adiabatic excitation energies to the $2\,^1A_g^-$ and $2\,^1A_1$ states can be observed experimentally (in particular for the *cis* isomer), and our results are in excellent agreement with the experimental values. On the contrary, the vertical excitation energies for these states are not directly observable in the experimental spectra and the "experimental" values are obtained by educated guesses. We show that the hypotheses underlying these guesses are not entirely grounded.

1 Introduction

The ab initio study of small conjugated polyenes is a nontrivial issue. For molecules like ethene, butadiene, and hexatriene several aspects complicate the study of the spectroscopic properties, namely the presence of excited states in a narrow energetic gap with very different natures (Rydberg, ionic, given by a HOMO–LUMO transition, or covalent, with a multireference nature) and their equilibrium geometries, which can belong to a symmetry point group different from that of the ground state (GS) as a consequence of the loss of planarity.

The ground state geometry of all-trans polyenes belongs to the C_{2h} point group, the ground state is indicated with $1\,^1A_g^-$, and the first singlet excited states are labeled $2\,^1A_g^-$ and $1\,^1B_u^+$. The labels "plus" and "minus" refer to the so-called particle–hole pseudosymmetry [1–3]. The occupied orbitals are numbered from the highest one down (using the index

i) and the virtual orbitals from the lowest one up (index i') and the orbitals i, i' are called a conjugated pair. In an independent particle model, assuming the occupied and virtual orbital energies to be symmetrically disposed ($\epsilon_{i'} = -\epsilon_i$), the energy of the configuration obtained by a $i \to j'$ excitation is equal to that obtained from a $j \to i'$ excitation. The linear combinations of the two degenerate configurations generate the minus and the plus states [2]. Moreover, one can show that the GS and the closed-shell determinants have a minus symmetry and that the intrapair $i \to i'$ single excitations have a plus symmetry. Minus and plus symmetry gives an important indication of the nature of the states: The minus states are dominated by neutral (or covalent) electronic distributions, while plus states have essentially an ionic nature [4]. The analysis of the nature of these states in linear polyenes and in more complex conjugated hydrocarbon molecules becomes evident when they are described using localized orbitals [5–11] within the frame of the orthogonal valence bond approach [12–15]. Finally, the interaction between minus and plus states is vanishing and the dipole transition moment is different from zero only between states of different minus/plus symmetry.

The relative ordering of these excited states in polyenes is matter of discussion, since a definitive conclusion has not been reached in the literature. The generally accepted scheme is that for hexatriene and octatetraene the $2\,^1A_g^-$

✉ Celestino Angeli
anc@unife.it

1   Charles River Laboratories, Chesterford Research Park, Saffron Walden CB10 1XL, UK

2   Dipartimento di Scienze Chimiche, Farmaceutiche e Agrarie, Università di Ferrara, Via Borsari 46, 44121 Ferrara, Italy

and $1\,^1B_u^+$ states are almost degenerate [2, 16, 17], while for longer polyenes $2\,^1A_g^-$ is the first excited state.

For all linear conjugated polyenes in the C_{2h} geometry, the one photon transition $2\,^1A_g^- \leftarrow 1\,^1A_g^-$ is dipole forbidden by symmetry (both for the $g \rightarrow g$ and for the particle–hole pseudosymmetry selection rules). On the other hand, the HOMO→LUMO transition to the $1\,^1B_u^+$ state is allowed and it leads to an intense absorption in the experimental spectrum. Since the $2\,^1A_g^-$ and $1\,^1B_u^+$ states are in general close in energy this strong absorption prevents any possible experimental observation (in violation of the selection rule) of the $2\,^1A_g^- \leftarrow 1\,^1A_g^-$ weak transition [18, 19]. It is known that the $1\,^1B_u^+$ excited state is nonfluorescent in hexatriene, while octatetraene exhibits two fluorescent emissions, without an energy gap between the absorption and the emission spectra in gas phase [20, 21] (both processes involve the GS and the $1\,^1B_u^+$ state). The absence of fluorescence in hexatriene can be justified considering the presence of conical intersections close to the Franck–Condon region, which can lead to the quick depopulation of the $1\,^1B_u^+$ state. For hexatriene, the depopulation of the $1\,^1B_u^+$ state is supposed to be induced by a totally symmetric displacement toward the $1\,^1B_u^+$–$2\,^1A_g^-$ crossing, which involves simultaneous expansion of the double bonds and contraction of the single bond lengths. From this region in the PES another radiationless decay to the ground state follows as a consequence of the vibration along non-totally symmetric natural coordinates. Within this model, $2\,^1A_g^-$ is lower in energy than $1\,^1B_u^+$. The radiationless decay is consistent with the non-planar geometry of the $2\,^1A_g^-$ state where the rotations and vibrations are expected to be very easily performed. This distortion is common for short polyenes but it is less pronounced with an increasing number of double bonds, where the π conjugation is preserved [22]. The energy gap between the two states increases with the polyene lengths, suggesting that internal conversion between them should be faster in shorter polyenes [23].

From the theoretical point of view different features of the $2\,^1A_g^-$ and $1\,^1B_u^+$, low-lying singlet excited states complicate their study: A double excitation has a consistent weight in $2\,^1A_g^-$; therefore, this state is in principle poorly described by linear response methods, applied, for instance, on the coupled cluster (CC), EOM-CC, or DFT approaches, while for an accurate description of the $1\,^1B_u^+$ ionic excited state different complex effects must be taken into account, such as dynamic σ polarization [24–26] and the contraction of the p atomic orbitals on the carbon atoms [27]. For these reasons, the balanced description of states of different nature, ionic and covalent in this case, is a computational challenge [25, 28]. In summary, a delicate equilibrium is required between the computational cost and the requirement to have a satisfying and balanced

inclusion of both the static and dynamic electron correlation. In this paper, it is worth recalling shortly the contributions of M. Persico in the field of the developments of methods aiming to effectively compute electronic states [29–31], to identify a diabatic representation of these states [10, 32–34] and to perform the simulation of photochemical processes [35–42].

The spectroscopic properties of *cis*-hexatriene are similar to those of the trans isomer discussed before. The $2\,^1A_1$ excited state reproduces the same behavior as the $2\,^1A_g^-$ state in the *trans* isomer and the $1\,^1B_2$ state that of the $1\,^1B_u^+$ state. The only difference is that in the cis isomer the absence of an inversion center formally allows the optic transition $2\,^1A_1 \leftarrow 1\,^1A_1$, that is however very weak. Also in this system, the complete lack of fluorescence is described in terms of crossing of the excited state surfaces.

The remainder of this paper is organized as follows: In Sect. 2, the computational details are described, and in Sect. 3, general considerations concerning the geometries here used for the ground states and the vertical excitation energies are discussed. The equilibrium geometries of the excited states of the two isomers of hexatriene and the adiabatic and emission energies are described in Sect. 4. A few general comments on the comparison of the results here obtained with the experimental data are presented in Sect. 6. Finally, in Sect. 6 some conclusive remarks are reported.

2 Computational details

All calculations here discussed are performed with the ANO basis set with contraction $(14s9p4d)/[4s3p1d]$ on the carbon atoms and $(8s4p)/[2s1p]$ on the hydrogen atoms. In order to check the dependence of the results on the basis set, the calculations have been performed also with the cc-pVTZ basis set [43], with contraction $(10s5p2d1f)/[4s3p2d1f]$ on the C atoms and $(5s2p1d)7[3s2p1d]$ on the H atoms. For the sake of conciseness and given that they do not modify the description obtained with the ANO basis set, the cc-pVTZ results are reported in Supplementary Information. The complete active space self-consistent field (CASSCF) and complete active space second-order perturbation theory [44–47] (CASPT2) calculations have been performed with the MOL-CAS suite of programs [48, 49] and the n-electron valence state perturbation theory (NEVPT2) calculation with a code developed in our laboratory [50–54] and interfaced to the MOLCAS suite. The active orbitals of the CASSCF wave functions belong in all cases to the π manifold. The active space is here indicated with CAS $(6,M)$ with M indicating the number of active orbitals where the 6 active electrons are distributed. The trend of the vertical and non-vertical adsorptions is studied expanding the active space from 6

to 14 active orbitals, and the same approach is used for the emission energies. The geometries obtained at the CASSCF level are compared, when possible, with those resulting from an optimization at the NEVPT2 level performed with the ORCA program [55].

The ground state of *trans*-hexatriene is described within the C_{2h} planar geometry, while the ground state of *cis*-hexatriene within the C_{2v} planar geometry. In CAS (6,M), the M active orbitals are distributed in the (a_g, a_u, b_u, b_g) irreps of the C_{2h} symmetry group (*trans*-hexatriene) as $(0, \frac{M}{2}, 0, \frac{M}{2})$ and in the (a_1, a_2, b_1, b_2) irreps of the C_{2v} symmetry group (*cis*-hexatriene) as $(0, \frac{M}{2}, \frac{M}{2}, 0)$.

The CASSCF description is perturbatively corrected using the NEVPT2 approach [50–53], by computing the second-order correction to the energy with the quasi-degenerate [54] (QD-NEVPT2) approach. Two different partitions of the Hamiltonian, strongly contracted, SC, and partially contracted, PC (QD-SC2 and QD-PC2 for the quasi-degenerate formulation), have been implemented within the NEVPT2 method, both use the Dyall Hamiltonian [56] to define the zeroth-order energies, while the level of contraction in the first-order interacting space (FOIS) is different. In particular, the FOIS in PC-NEVPT is larger than in SC-NEVPT and it is equal to the one used in CASPT2 [44–47]. The QD-NEVPT2 results are compared to those obtained at the multi-state CASPT2 (MS-CASPT2) level [57]. MS-CASPT2 calculations have been performed with a real level shift [45, 47] of 0.3 *hartree* to mitigate the intruder state problem and using both the original partition of the Hamiltonian [44, 45] and the modification [46] proposed in 2004, in which the IPEA parameter has been introduced, setting its value to 0.25 hartree. These two variants of CASPT2 are hereafter indicated with "IPEA = 0" and "IPEA = 0.25," respectively.

Table 1 Bond lengths (Å) and angles (degrees) for the $1\,^1A_g^-$ state of *trans*-hexatriene optimized at the CASSCF(6,6) and CASSCF(6,6)/NEVPT2 levels

Parameter	$1\,^1A_g^-$	
	CASSCF	NEVPT2
C_1–C_2	1.344	1.342
C_2–C_3	1.458	1.448
C_3–C_3'	1.348	1.349
C_1–H_1	1.075	1.078
C_1–H_2	1.077	1.082
C_2–H_3	1.078	1.085
C_3–H_4	1.079	1.086
$\theta(C_1C_2C_3)$	124.19	123.61
$\theta(C_2C_3C_3')$	123.97	123.86
$\theta(H_1C_1H_2)$	117.03	117.21
$\theta(C_3C_2H_3)$	116.69	116.90

3 Vertical excitations

As a first step, the dependence of the vertical excitation energies on the computational parameters has been investigated. To this aim, we focus on the vertical excitation energies for the $2\,^1A_g^-$, $1\,^1B_u^+$, and $2\,^1B_u^-$ states of *trans*-hexatriene and for the $2\,^1A_1$, $1\,^1B_2$, and $2\,^1B_2$ states of *cis*-hexatriene. The vertical excitations are computed at the CASSCF (6,6) and CASSCF(6,6)/NEVPT2 optimized geometries. As it will be discussed in Sects. 3.1 and 3.2, the ground state optimal geometry is almost the same at the two levels of theory. Therefore, the vertical excitations are not expected to show a marked dependence on the method used to optimize the geometry.

3.1 *trans*-hexatriene

The main geometrical parameters of *trans*-hexatriene are reported in Table 1 (the C atoms are numbered from the extremities to the center of the molecule, so that C_1 and C_1' are the two terminal C atoms, see Fig. 1). One promptly notes that the two geometries are close to each other. For a comparison with the values obtained with the cc-pVTZ basis set, a full description of the equilibrium geometry (in cartesian coordinates), and the values of the harmonic frequencies at the equilibrium geometry, see Tables S.1, S.2, and S.3 of Suppl. Inform., respectively.

The vertical excitation energies for the $2\,^1A_g^- \leftarrow 1\,^1A_g^-$ transition are reported in Table 2. The computed values do not vary significantly with the enlargement of the active space (moving from 6 to 14 active orbitals) and with the method used to optimize the geometry. At the CASSCF level, the excitation energy is in the range 5.54–5.65 eV and the effect of the electron correlation introduced by the perturbation treatment is not very relevant, leading to values in the range 5.42–5.53 eV for MS-CASPT2 (5.17–5.24 with IPEA = 0), 5.55–5.68 eV with QD-SC2 and 5.52–5.65 eV with QD-PC2. For this reason, we can
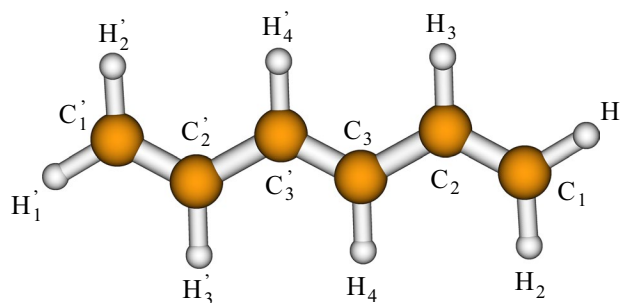

Fig. 1 Atom numbering for *trans*-hexatriene

say that the GS and the $2\,^1A_g^-$ states are described at a very similar level by the CASSCF functions, since the perturbation correction on the energy differences is not large (in particular at NEVPT2 level). Using the standard CASPT2 zeroth-order Hamiltonian (IPEA = 0.25) [46], the transition energies are closer to the values computed with QD-NEVPT2 and are 0.2–0.3 eV higher than the CASPT2 (IPEA = 0) results. This is a well-known behavior of the CASPT2 transition energies [46] with the two different zeroth-order Hamiltonians (see, for instance, Ref. [58–60] for some specific cases). The partition of the Hamiltonian based on the IPEA = 0.25 value is considered more reliable, even if this value has been brought into question, both in the description of organic molecules [61, 62] and of molecules containing transition metals [63, 64]. The results of the present study confirm that the IPEA = 0.25 zeroth-order Hamiltonian gives better results than the IPEA = 0.0 one. The theoretical accepted value for this transition is 5.19 eV, obtained in a CASPT2 study. This result has been published [65] in 1993 before the introduction of the IPEA = 0.25 zeroth-order Hamiltonian. This value has been assumed as a benchmark theoretical value for this transition since it reproduces the experimental value [16] (5.21 eV) published in 1985.

Indeed, the two-photon transition to $2\,^1A_g^-$ is not forbidden (even if it is very weak) but the assignment [16] of a maximum at 5.21 eV is not obvious, in particular if one considers the low intensity of the bands [66]. It is worth noticing that in the theoretical study of excited states one normally compares the computed vertical transition energies with the energy of the maximum in the absorption spectra. This approach is based on the implicit assumption that there is a significant geometrical displacement passing from the equilibrium geometry of the GS to that of the excited state, so that the vibrational wave function of the excited state with the maximum Franck–Condon factor has an energy for which one of the classic turning points is close to the equilibrium geometry of the ground state (for high vibrational quantum numbers the largest value of the wave functions is in the region of the classical turning points). However, this assumption does not always hold and the absorption maximum can be at a different energy than the vertical excitation.

Moreover, the experimental value for the vertical excitation energy for this transition has not been unequivocally defined. Indeed, warnings are reported in Ref. [16] concerning the reported values. In particular, the authors state that "the present method is prone to larger error in the region of small absorptivity" and that "some remarkable structures in the main band region appear to indicate the difference between both isomers, but are not accurate enough to be analyzed to locate the 0–0 origin." The experimental knowledge on hexatriene has been summarized by McDiarmid [67] in 1999 in a study on the electronic spectra of small linear polyenes where it is explicitly stated that "the FC energies of the $2\,^1A_g^- \leftarrow 1\,^1A_g^-$ transitions are, therefore, experimentally unknown." In the same work, possible values for the vertical excitation energies of these systems are proposed, but one must bear in mind that these are not true experimental values, but rather values obtained starting from the experimental data using (reasonable) hypotheses. At this point, it is worth stressing that there is an unambiguous value which can be obtained from the experimental spectrum, the 0–0 (adiabatic) transition energy [67–69] for the analogous state of *cis*-hexatriene, and this value is 4.26 eV. This aspect is fully discussed in Sect. 4.2, and here, we limit ourselves to highlight that a true experimental value for the $2\,^1A_g^- \leftarrow 1\,^1A_g^-$ vertical transition is not available.

The importance of a reliable value for the vertical transition energy of the $2\,^1A_g^-$ state of *trans*-hexatriene (and other small polyenes) should not be underestimated. Indeed, besides its key role in the interpretation of the spectroscopy behavior, the complex nature of this state (with a large content of a double excitation) makes its vertical excitation energy a critical test case for new approaches aiming to overcome the restrictions of methods where only singly excited state are well described (such as, in general, the linear response methods), as already pointed out for same state of octatetraene [17]. In these studies (see Refs. [10, 59, 70–81] for a non-exhaustive list of recent examples), the use of a reliable reference value is of paramount importance.

The good agreement of the MS-CASPT2 (IPEA = 0.25) values with those of NEVPT2 (both SC and PC) and the very

Table 2 Vertical excitation energies (eV) for the $2\,^1A_g^-$ state of *trans*-hexatriene computed at the CASSCF (6,*M*), MS-CASPT2(IPEA = 0.25), QD-NEVPT2 (QD-SC2 and QD-PC2) levels using the CASSCF and NEVPT2 geometries (see text)

	$2\,^1A_g^- \leftarrow 1\,^1A_g^-$			
	CASSCF	MS-CASPT2	QD-SC2	QD-PC2
CASSCF(6,6) geometry				
CAS (6,6)	5.629	5.529(5.213)	5.682	5.652
CAS (6,8)	5.646	5.510(5.228)	5.657	5.624
CAS (6,10)	5.645	5.484(5.233)	5.647	5.613
CAS (6,12)	5.601	5.463(5.233)	5.602	5.569
CAS (6,14)	5.592	5.460(5.241)	5.595	5.558
NEVPT2 geometry				
CAS (6,6)	5.579	5.488(5.174)	5.640	5.610
CAS (6,8)	5.596	5.469(5.190)	5.616	5.583
CAS (6,10)	5.596	5.443(5.195)	5.606	5.571
CAS (6,12)	5.550	5.424(5.195)	5.559	5.527
CAS (6,14)	5.543	5.420(5.202)	5.552	5.517

Values in brackets refer to CASPT2(IPEA = 0)

small dependence on small variations of the geometrical parameters and on the enlargement of the active space allow us to indicate for the $2\,^1A_g^- \leftarrow 1\,^1A_g^-$ vertical transition energy the values 5.4 eV (CASPT2) and 5.5–5.6 eV (NEVPT2), values higher than the generally accepted one [16] (5.21 eV). The use of the cc-pVTZ basis set (see Table S.4 of Suppl. Inform.) gives very similar results (in average the transition energies increases by less than 0.1 eV). The comparison of the findings here obtained with previously published theoretical results and a comment on their relationship with the experimental observations is reported in Sect. 5.

For the ^1B_u symmetry, two states are close in energy ($1\,^1B_u^+$ and $2\,^1B_u^-$) and they are treated together using the quasi-degenerate PT formalism. The results are reported in Table 3. In agreement with what observed for $2\,^1A_g^-$ state the results obtained with the two different optimized geometries do not show substantial variations, unlike what reported for the bright state of other conjugated organic systems (see, for instance, Refs. [60, 82]). For other aspects, the $1\,^1B_u^+$ state shows different trends with respect to the $2\,^1A_g^-$ state. Indeed, the enlargement of the active space leads to a constant lowering of the $1\,^1B_u^+ \leftarrow 1\,^1A_g^-$ vertical excitation energy at the CASSCF level, passing from 7.3 eV for CAS (6,6) to 6.3–6.4 eV for CAS (6,14). The introduction of the dynamic electron correlation in a MRPT2 scheme leads to a marked reduction of the vertical excitation energy, thus showing that (as expected) the dynamic electron correlation is larger for the ionic $1\,^1B_u^+$ state than for the neutral $1\,^1A_g^-$ ground state. Moreover, the MRPT2 excitation energy increases with the enlargement of the active space, with a moderate variation at the MS-CASPT2 level (from 5.3 to 5.4 eV; from 4.9 to

5.2 eV with IPEA = 0.0) and a more marked variation at the QD-SC2 (from 4.8 to 4.9 eV to 5.6 eV) and QD-PC2 (from 4.7 to 5.5 eV) levels. It is also worth noticing that, with 6, 8, 10 active orbitals the two ^1B_u states are not correctly ordered at the CASSCF level. Indeed, a second excited state of the same symmetry ($2\,^1B_u^-$, a neutral state) is placed above the ionic $1\,^1B_u^+$ state. With the minimum active space, the two roots are inverted at the CASSCF level. This is of course an artifact due to the lack of the electron correlation, a deficiency which is reduced by enlarging the active space [25]. With the CAS(6,12) and CAS(6,14) active spaces the two ^1B_u states have the correct ordering at the CASSCF level. One can note that the vertical excitation energies to the $2\,^1A_g^-$ and $1\,^1B_u^+$ excited states computed at the highest levels (MRPT2 on the CAS (6,14) CASSCF wave functions) are almost degenerate: $\simeq 5.4$ eV with MS-CASPT2(IPEA = 0.25) ($\simeq 5.4$ eV; $\simeq 5.2$ eV with IPEA = 0.0), $\simeq 5.6$ eV with QC-SC2 and $\simeq 5.5$ with QC-PC2. As found for the $2\,^1A_g^-$ state, the use of the cc-pVTZ basis set (see Table S.5 of Suppl. Inform.) gives very similar results with an increase of the transition energies of by 0.1–0.15 eV. These results indicate that the two states are virtually degenerate in the Franck–Condon zone.

Finally, it is worth highlighting that also for this transition, the experimental reference value [83–85] ($\simeq 4.9$ eV) concerns the 0–0 transition (it is the most intense in the vibrational progression) and it is considered as a reference for the vertical excitation under the assumption that the vertical and adiabatic excitation energies coincide. The evidence of the present study (see also Sect. 4.1) indicates that also for this state care must be exerted when the maximum

Table 3 Vertical excitation energies (eV) for the $1\,^1B_u^+$ state of *trans*-hexatriene computed at the CASSCF (6,M), MS-CASPT2(IPEA = 0.25), QD-NEVPT2 (QD-SC2 and QD-PC2) levels using the CASSCF and NEVPT2 geometries (see text)

	$1\,^1B_u^+ \leftarrow 1\,^1A_g^-$				$2\,^1B_u^- \leftarrow 1\,^1A_g^-$			
	CASSCF	MS-CASPT2	QD-SC2	QD-PC2 2	CASSCF	MS-CASPT2	QD-SC2	QD-PC2 2
CASSCF(6,6) geometry								
CAS (6,6)	6.859	5.300(4.901)	4.876	4.708	6.807	6.579(6.161)	6.769	6.735
CAS (6,8)	6.920	5.337(4.938)	5.377	5.274	6.667	6.679(6.452)	6.671	6.686
CAS (6,10)	6.761	5.343(5.031)	5.522	5.394	6.611	6.530(6.324)	6.587	6.611
CAS (6,12)	6.508	5.339(5.107)	5.591	5.427	6.619	6.534(6.319)	6.560	6.554
CAS (6,14)	6.381	5.389(5.187)	5.646	5.507	6.604	6.504(6.289)	6.541	6.544
NEVPT2 geometry								
CAS (6,6)	7.272	5.263(4.861)	4.846	4.676	6.786	6.560(6.147)	6.747	6.713
CAS (6,8)	6.895	5.307(4.915)	5.348	5.245	6.630	6.657(6.429)	6.649	6.663
CAS (6,10)	6.725	5.301(4.991)	5.499	5.364	6.575	6.517(6.315)	6.554	6.583
CAS (6,12)	6.468	5.319(5.093)	5.558	5.398	6.593	6.504(6.287)	6.540	6.530
CAS (6,14)	6.342	5.363(5.165)	5.615	5.478	6.579	6.478(6.263)	6.518	6.520

Values in brackets refer to CASPT2 performed with IPEA = 0

in the adsorption spectrum is directly compared with the vertical excitation energy.

Also in this case, the comparison of the findings here obtained with previously published theoretical results and their relationship with the experimental observations is reported in Sect. 5.

3.2 *cis*-hexatriene

The parameters for the equilibrium geometry of the ground state of *cis*-hexatriene computed at the CASSCF(6,6) and the CASSCF(6,6)/NEVPT2 level within the C_{2v} symmetry point group are reported in Table 4. The C atoms are numbered as for the *trans* isomer, see Fig. 2. For a comparison with the values obtained with the cc-pVTZ basis set, a full description of the equilibrium geometry (in cartesian coordinates), and the values of the harmonic frequencies at the equilibrium geometry, see Tables S.6, S.7, and S.8 of Suppl. Inform., respectively.

As mentioned in Sect. 1, even if the transition to the $2\,^1A_1$ state is formally dipole allowed, its oscillator strength is so small that it cannot be observed. It is possible to reach this state in a two-photon experiment, but it is difficult to identify a possible value for the vertical excitation energy (see the comments reported in Sect. 3.1). From the experimental point of view [67–69], the 0–0 transition energy can be identified without ambiguities and its value is 4.26 eV. The vertical excitation energy is expected to be markedly higher, given the important variation of the $2\,^1A_1$ energy when passing from the FC region to the $2\,^1A_1$ equilibrium geometry (see Sect. 4.2).

The vertical excitation energies to the $2\,^1A_1$ state computed in the present work are listed in Table 5. *Ab initio* calculations performed at the CASPT2 level identify the vertical $2\,^1A_1 \leftarrow 1\,^1A_1$ transition at 5.04 eV [86] and it is relevant to stress that this result has been obtained before the introduction of the IPEA = 0.25 modification of the zeroth-order Hamiltonian. Our CASPT2 values with IPEA = 0 are
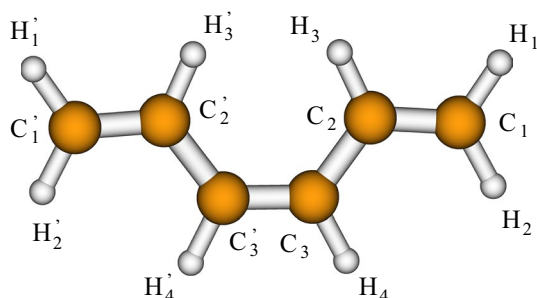
close to this value, which is increased to ≃5.4 eV when the IPEA = 0.25 zeroth-order Hamiltonian is used.

The results in Table 5 closely recall what observed for the vertical transition to the $2\,^1A_g^-$ state of the *trans* isomer. Indeed, at all levels of calculation one notes a small dependence of the computed values on the dimension of the active space and on the method used to optimize the ground state geometry. Moreover, NEVPT2 (both flavors) and CASPT2 (with IPEA = 0.25) give rather close values. Finally, the MRPT2 values are in general close (or very close for the largest active spaces) to the CASSCF values, thus

Table 4 Bond lengths (Å) and angles (degrees) for the $1\,^1A_1$ state of *cis*-hexatriene optimized at the CASSCF(6,6) and CASSCF(6,6)/NEVPT2 levels

Parameter	$1\,^1A_1$	
	CASSCF	NEVPT
C_1-C_2	1.344	1.342
C_2-C_3	1.461	1.450
C_3-C_3'	1.351	1.352
C_1-H_1	1.075	1.080
C_1-H_2	1.077	1.081
C_2-H_3	1.075	1.083
C_3-H_4	1.077	1.084
$\theta(C_1C_2C_3)$	123.31	122.72
$\theta(C_2C_3C_3')$	127.04	126.49
$\theta(H_1C_1H_2)$	117.00	117.21
$\theta(C_3C_2H_3)$	118.20	118.47

Table 5 Vertical excitation energies (eV) for the $2\,^1A_1$ state of *cis*-hexatriene computed at the CASSCF (6,*M*), MS-CASPT2(IPEA = 0.25), QD-NEVPT2 (QD-SC2 and QD-PC2) level using the CASSCF and NEVPT2 geometries

	$2\,^1A_1 \leftarrow 1\,^1A_1$			
	CASSCF	MS-CASPT2	QD-SC2	QD-PC2
CASSCF(6,6) geometry				
CAS (6,6)	5.651	5.514(5.179)	5.682	5.648
CAS (6,8)	5.596	5.461(5.164)	5.546	5.516
CAS (6,10)	5.581	5.466(5.200)	5.545	5.514
CAS (6,12)	5.554	5.408(5.168)	5.544	5.506
CAS (6,14)	5.550	5.401(5.174)	5.521	5.484
NEVPT2 geometry				
CAS (6,6)	5.597	5.467(5.134)	5.635	5.601
CAS (6,8)	5.536	5.413(5.118)	5.495	5.465
CAS (6,10)	5.523	5.419(5.156)	5.494	5.463
CAS (6,12)	5.497	5.361(5.123)	5.494	5.457
CAS (6,14)	5.495	5.354(5.128)	5.472	5.435

Values in brackets refer to CASPT2 performed with IPEA = 0

Fig. 2 Atom numbering for *cis*-hexatriene

indicating that the dynamic correlation of the electrons is very similar for the two states, or, in other words, that the CASSCF description of the two states is well balanced. It is worth noticing that following the classification reported in Sect. 1 both states involved in the transition are neutral. These results allow to indicate for the $2\,^1A_1 \leftarrow 1\,^1A_1$ vertical transition energy the values 5.4 eV (CASPT2) and 5.4–5.5 eV (NEVPT2), very close to the values found for *trans*-hexatriene. The use of the cc-pVTZ basis set (see Table S.9 of Suppl. Inform.) gives very similar results, only slightly higher by 0.05–0.10 eV. These results are further discussed in Sect. 5.

The vertical excitation energies for the $1\,^1B_2 \leftarrow 1\,^1A_1$ transition are reported in Table 6 (see Table S.10 of Suppl. Inform. for the values with the cc-pVTZ basis set). Also for this state a behavior analogous to that found for the *trans* isomer is observed. Indeed, the first two states ($1\,^1B_2$ and $2\,^1B_2$) in this symmetry are close in energy, thus requiring the use of the quasi-degenerate version of PT2. The CAS-SCF transition energy to the $1\,^1B_2$ state shows a gradual lowering when the active space is enlarged (with an inversion of the order of the two states for all active spaces) and the opposite behavior is in general found for the PT2 values (this is more clear at the NEVPT2 level). Passing from the CASSCF to the PT2 description one notes a marked lowering of the vertical excitation energy, showing that the ionic $1\,^1B_2$ state has a larger dynamic electron correlation than the neutral $1\,^1A_1$ state. Finally, the best values for the $1\,^1B_2$ vertical excitation energy (those obtained with the largest active space) are 5.4 eV (CASPT2(IPEA = 0.25); 5.2 with IPEA = 0.0) and 5.5–5.6 eV (NEVPT2), very close to the values

obtained for the $2\,^1A_1$ state. The $1\,^1B_2$ and $2\,^1A_1$ states are therefore virtually degenerate. These results are discussed in Sect. 5.

4 Excited state geometry optimizations, adiabatic transition energies, and vertical emission energies

In this section, we report the equilibrium geometries of the two relevant excited states for both isomers. This allows to compute the adiabatic excitations and vertical emission energies. The geometry optimization for these two states is not trivial, therefore ad hoc solutions must be used and they are hereafter described. When possible, the vibrational frequencies are obtained at the optimized geometry and in these cases the zero point vibrational energies (ZPE) are taken into account for the calculation of the adiabatic transition energies. Finally, vertical emission energies are computed at the optimized geometries of the excited states. As done for the vertical transition energies, the values obtained at different levels of theory, that is, CASSCF, MS-CASPT2, and QD-NEVPT2, are compared.

4.1 *trans*-hexatriene

The $2\,^1A_g^-$ state has been optimized firstly under the C_{2h} symmetry constraint. At this optimal geometry one imaginary frequency has been found. A rotation of the terminal CH_2 groups, which breaks the planarity of the molecule, induces a geometry relaxation that leads to a non-planar minimum

Table 6 Vertical excitation energies (eV) for the $1\,^1B_2$ and $2\,^1B_2$ states of *cis*-hexatriene computed at the CASSCF (6,*M*), MS-CASPT2 (IPEA = 0.25), QD-NEVPT2 (QD-SC2 and QD-PC2) levels using the CASSCF and NEVPT2 geometries

	$1\,^1B_2 \leftarrow 1\,^1A_1$				$2\,^1B_2 \leftarrow 1\,^1A_1$			
	CASSCF	MS-CASPT2	QD-SC2	QD-PC2	CASSCF	MS-CASPT2	QD-SC2	QD-PC2
CASSCF(6,6) geom.								
CAS (6,6)	6.833	5.297(4.890)	4.895	4.725	7.317	6.740(6.355)	6.899	6.878
CAS (6,8)	6.662	5.297(4.878)	5.298	5.179	6.921	6.739(6.343)	6.733	6.774
CAS (6,10)	6.604	5.359(5.058)	5.432	5.311	6.828	6.744(6.508)	6.786	6.794
CAS (6,12)	6.467	5.471(5.265)	5.569	5.442	6.799	6.683(6.412)	6.860	6.808
CAS (6,14)	6.408	5.436(5.148)	5.633	5.493	6.757	6.679(6.366)	6.757	6.747
	CAS	MS-CASPT2	QD-SC2	QD-PC2	CAS	MS-CASPT2	QD-SC2	QD-PC2
NEVPT2 geom.								
CAS (6,6)	6.812	5.259(4.852)	4.862	4.689	7.281	6.725(6.342)	6.884	6.864
CAS (6,8)	6.758	5.305(4.916)	5.263	5.146	6.888	6.812(6.583)	6.717	6.757
CAS (6,10)	6.562	5.342(5.052)	5.396	5.280	6.803	6.719(6.476)	6.776	6.778
CAS (6,12)	6.428	5.442(5.241)	5.531	5.408	6.775	6.667(6.393)	6.843	6.792
CAS (6,14)	6.370	5.409(5.204)	5.598	5.462	6.736	6.660(6.423)	6.743	6.732

Values in brackets refer to CASPT2 performed with IPEA = 0

with all vibrational frequencies being real. The C_{2h} minimum is a saddle point between two minima of C_2 and C_s symmetries. However, the imaginary frequency is very small (the surface along this normal mode is rather flat). Similar results have been obtained also with the cc-pVTZ basis set. In previous studies [25], this state has been optimized within the C_2 symmetry. The carbon skeleton is almost identical to the minimum C_{2h} structure and only one of the two terminal hydrogens is out of the molecular plane by 14 degrees [25].

In the non-symmetric optimized geometry, obtained in this work, the H1–C1–C2–H3 atoms form a dihedral angle of 7.63 degrees. This result has been obtained with a CASSCF geometry optimization. When the angle is reduced to zero by mean of a rigid rotation around the C–CH$_2$ bond, the CASSCF energy for the state is essentially the same (the energy variation is lower than 0.01 eV). Given the quasi degeneracy between the two structures the topology of the PES for the $2\,^1A_g^-$ state in the region around the energy minimum may change by minor changes in the computational strategy (basis set, active space, etc.). So it is not clear whether the true minimum is planar or not [25].

In our opinion, the detailed description of the topology of the PES around the minimum is not really relevant to understand the spectroscopic behavior of this system, while it is very important to describe the photochemical fate of a molecule reaching this region. It is worth recalling that in presence of a flat PES along a normal coordinate, the concept of nuclear geometry loses relevance given that the nuclear wave function is more delocalized than in the case of a potential

with a marked increase moving from the minimum (as the harmonic potential). Moreover, in such a case the harmonic approximation cannot be applied. These considerations suggest a reasonable (and simplified) computational approach for the adiabatic excitation energies based on the imposition of a C_{2h} equilibrium geometry for the $2\,^1A_g^-$ excited state.

The geometrical parameters of the equilibrium geometry of the $2\,^1A_g^-$ state are reported in Table 7 for a full optimization without symmetry constraint (at CASSCF and NEVPT2 levels) and with the C_{2h} symmetry constraint (CASSCF). The results show that the NEVPT2 optimized geometry is very close to the CASSCF one and that the symmetry constraint has practically no effect on the main geometrical parameters. In both the $1\,^1A_g^-$ and $2\,^1A_g^-$ states there is a clear distinction between single and double bonds, but in the $2\,^1A_g^-$ state they are reversed with respect to the ground state. This consideration allows to understand why the rotation around the terminal C–CH$_2$ bonds can occur in the $2\,^1A_g^-$ state: After the bond order inversion the terminal bond is a single bond and the rotation around it is almost barrierless.

The main geometrical values obtained with the cc-pVTZ basis set, a full description of the equilibrium geometry (in cartesian coordinates), and the values of the real harmonic frequencies at the equilibrium geometry of the $2\,^1A_g^-$ state, are reported in Tables S.11, S.12, and S.13 of Suppl. Inform., respectively.

The adiabatic transition energies (0–0 transitions) for the $2\,^1A_g^-$ state are reported in Table 8 using the CASSCF and NEVPT2 fully optimized (no symmetry constraint) $2\,^1A_g^-$ equilibrium geometries. All considerations reported for the $2\,^1A_g^- \leftarrow 1\,^1A_g^-$ vertical transition energy of *trans*-hexatriene, concerning the dependence on the active space dimension, on the geometry and on the MRPT2 method, are valid also for this case. One promptly notes that these values are significantly lower than the vertical excitation energies (see Table 2). This indicates that the energy of the $2\,^1A_g^-$ state decreases considerably moving from the equilibrium geometry of the ground state to the optimized minimum on its PES. Focusing on the largest active space, this difference is as large as 1.0 eV (CASPT2) and 1.0–1.1 eV (NEVPT2). Once the zero point vibrational energy correction for the two states, Δ(ZPVE), is considered, the difference between the vertical and the adiabatic excitations is about 1.2 eV (CASPT2) and 1.2–1.3 eV (NEVPT2), in good agreement with the early estimation (1.2 eV) of Cave and Davidson [87].

Concerning the comparison of the present results with the experimental observations, we highlight again that this comparison is not trivial. In 1990 Buma et al have performed an experimental study [69] to locate the $2\,^1A_g^-$ state for *trans*-hexatriene and *cis*-hexatriene and they stated that

Table 7 Bond lengths (Å) and angles (degrees) for the $2\,^1A_g^-$ state of *trans*-hexatriene obtained without any symmetry constraint (at CASSCF and NEVPT2 levels) and with the C_{2h} symmetry constraint (CASSCF)

Parameter	$2\,^1A_g^-$		
	No symmetry		C_{2h}
	CASSCF	NEVPT2	CASSCF
C_1-C_2	1.467	1.455	1.467
C_2-C_3	1.387	1.379	1.387
C_3-C_3'	1.436	1.434	1.437
C_2'–C_3'	1.387	1.379	1.387
C_1'–C_2'	1.467	1.455	1.467
C_1–H_1	1.072	1.078	1.072
C_1–H_2	1.074	1.079	1.074
C_2–H_3	1.076	1.085	1.076
C_3–H_4	1.078	1.085	1.078
$\theta(C_1C_2C_3)$	124.03	123.69	124.05
$\theta(C_2C_3C_{3'})$	124.28	124.00	124.26
$\theta(H_1C_1H_2)$	118.44	118.43	118.52
$\theta(C_3C_2H_3)$	118.77	118.54	118.76

Table 8 Adiabatic excitation energies (eV) for the $2\,^1A_g^- \leftarrow 1\,^1A_g^-$ transition of *trans*-hexatriene computed at the CASSCF(6,6) and NEVPT2 reference geometries (obtained without any symmetry constraint)

| | $2\,^1A_g^- \leftarrow 1\,^1A_g^-$ | | | |
	CASSCF	MS-CASPT2	QD-SC2	QD-PC2
CAS(6,6) geometry				
Δ (ZPVE)= −0.212 eV				
CAS (6,6)	4.170	4.261(3.945)	4.399	4.380
CAS (6,8)	4.193	4.247(3.963)	4.372	4.351
CAS (6,10)	4.200	4.224(3.962)	4.360	4.339
CAS (6,12)	4.191	4.209(3.967)	4.389	4.338
CAS (6,14)	4.156	4.210(3.979)	4.343	4.342
	CASSCF	MS-CASPT2	QD-SC2	QD-PC2
NEVPT2 geometry				
Δ (ZPVE)= −0.200 eV				
CAS (6,6)	4.206	4.256(3.929)	4.416	4.398
CAS (6,8)	4.227	4.240(3.947)	4.389	4.368
CAS (6,10)	4.232	4.202(3.942)	4.374	4.352
CAS (6,12)	4.223	4.192(3.957)	4.406	4.353
CAS (6,14)	4.193	4.195(3.952)	4.341	4.347

Δ (ZPVE) is included. CASPT2 values are computed with the IPEA = 0.25 zeroth-order Hamiltonian. Values in brackets refer to CASPT2 performed with IPEA = 0

for *trans*-hexatriene "limitations on our present signal-to-noise ratio have prevented us from making an unambiguous assignment of the origin, but we know that it must have an energy ≥ 34038 cm^{-1}," corresponding to 4.22 eV. The best value obtained in this study, CASPT2 and NEVPT2 on CAS(6,14), are in the range 4.20–4.35 eV (see Table 8), in very good agreement with the experimental finding.

Looking at the values obtained for the vertical emission energies (Table 9) it is possible to note also an important increase of the ground state energy proceeding from its optimized minimum to the equilibrium geometry of the excited state. This destabilization can be computed as the difference between the adiabatic excitation energy (without the Δ(ZPVE) term) and the vertical emission energy, obtaining 0.8–0.9 eV for the CASSCF geometry and 1.2 eV for the NEVPT2 geometry. This difference between the values at the two geometries comes from the fact that the small energy changes along some normal mode observed for the $2\,^1A_g^-$ PES (which makes the adiabatic transition energy almost independent on the method used to optimize the geometry) is not reproduced in the $1\,^1A_g^-$ PES, which is much higher in energy at the $2\,^1A_g^-$ NEVPT2 optimal geometry than at the $2\,^1A_g^-$ CASSCF optimal geometry.

The values computed with the cc-pVTZ basis set (see Tables S.14 and S.15 of Suppl. Inform.) show only minor variations (of the order or less than 0.1 eV) with respect to those here discussed.
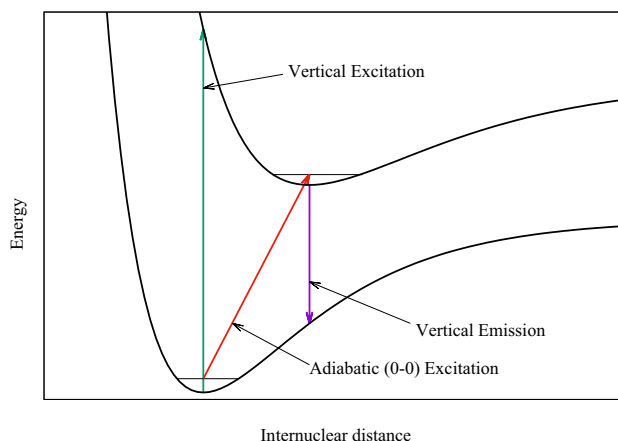

Fig. 3 Vertical excitation and emission energies (green and purple, respectively) and adiabatic 0–0 excitation energy (red) for a model diatomic molecule. The ground and the excited states are described by two Morse potentials

These results show that care must be taken when considering the "mirror image symmetry" [88] rule in which it is supposed that the difference between the adiabatic and the vertical excitation energies is the same as the difference between the adiabatic excitation and the vertical emission energies. This rule is often use to obtain "experimental" value for the vertical excitation energy [67, 88]
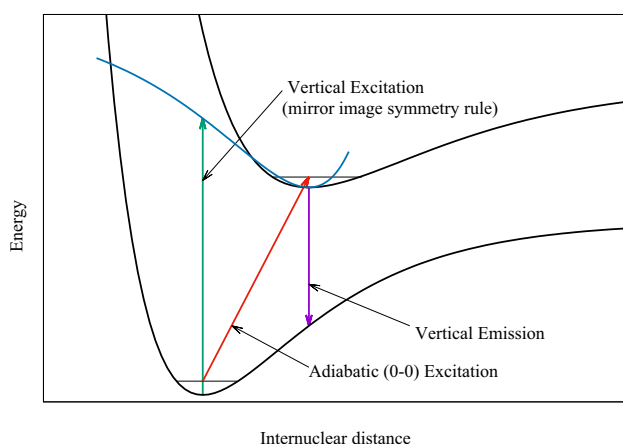
Fig. 4 Vertical excitation and emission energies (green and purple, respectively) and adiabatic 0–0 excitation energy (red) for a model diatomic molecule. The ground and the excited states are described by two Morse potentials. The vertical excitation energy is obtained using the mirror image symmetry rule, where the excited state energy curve at the left of its equilibrium geometry (for shorter internuclear distances, in blue in figure) is estimated by the mirror image of the ground state energy curve at the right of its equilibrium geometry (for larger internuclear distances)

Table 9 Vertical emission energies (eV) for the $1\,^1A_g^- \leftarrow 2\,^1A_g^-$ transition of *trans*-hexatriene calculated at the $2\,^1A_g^-$ CASSCF and NEVPT2 optimized geometries

	$1\,^1A_g^- \leftarrow 2\,^1A_g^-$			
	CASSCF	MS-CASPT2	QD-SC2	QD-PC2
CASSCF(6,6) geometry				
CAS (6,6)	3.519	3.636(3.400)	3.732	3.717
CAS (6,8)	3.520	3.628(3.414)	3.707	3.691
CAS (6,10)	3.506	3.615(3.419)	3.681	3.665
CAS (6,12)	3.525	3.607(3.422)	3.678	3.662
CAS (6,14)	3.509	3.608(3.432)	3.670	3.657
NEVPT2 geometry				
CAS (6,6)	3.168	3.274(3.047)	3.369	3.356
CAS (6,8)	3.167	3.265(3.060)	3.343	3.329
CAS (6,10)	3.150	3.248(3.063)	3.317	3.303
CAS (6,12)	3.168	3.240(3.072)	3.316	3.301
CAS (6,14)	3.165	3.239(3.069)	3.303	3.290

CASPT2 values are computed with the IPEA = 0.25 zeroth-order Hamiltonian. Values in brackets refer to CASPT2 performed with IPEA = 0

and one should bear in mind that in this case the "experimental vertical excitation energy" could have a considerable error [2, 17]. A schematic representation of the hazard related to the use of the mirror image symmetry rule is reported in Figs. 3 and 4. These figures are obtained for a model diatomic systems where the ground and the excited states are described by two Morse potentials and highlight the fact that the vertical excitation energy obtained with the mirror image symmetry rule can be lower than the actual vertical excitation energy.

On the other hand, all other considerations reported for the vertical transition energies to the $2\,^1A_g^-$ state (see the comments at Table 2 in Sect. 3.1) apply also for the vertical emission energies (Table 9).

The adiabatic transition energies and the vertical emission energies have been obtained also using the optimal C_{2h} CASSCF (6,6) equilibrium geometry for the $2\,^1A_g^-$ state. This strategy has been used in the past, see, for instance, Ref. [87]. Our results (see Tables S.14 and S.15 of Suppl. Inform.) indicate that values are very close to those obtained with the fully optimized geometry (the variation is limited to a few hundredths of an eV). Therefore, the use of the C_{2h} constraint in the geometry optimization, which implies a strong reduction of the computational cost of both the geometry optimization and the calculation of the excited state energies, modifies only marginally the results.

The spectroscopic experimental information available for the strongly allowed $1\,^1B_u^+ \leftarrow 1\,^1A_g^-$ transition is inadequate

to accurately establish the nature of upper state equilibrium geometry. However, the lack of a detectable fluorescence can be interpreted in terms of a substantially twisted equilibrium geometry for the $1\,^1B_u^+$ state.

A tendency toward an average bond lengths, intermediate between a single and a double bond, has been suggested [25, 89, 90]. Moreover the central bond seems to become formally a single bond and in this case it is reasonable to ask whether a planar structure could represent a true minimum for this state. The rotation around the central bond can be assumed as the main mechanism involved in the quenching of fluorescence.

From the computational point of view, the geometry optimization of the $1\,^1B_u^+$ state is more difficult than for the $2\,^1A_g^-$ state. Indeed, the two lowest states of B_u symmetry are in general mixed at CASSCF level and therefore the relative order of the roots can vary during the optimization procedure (root flipping problem). Moreover, the $1\,^1B_u^+$ state is virtually degenerate with the $2\,^1A_g^-$ state: For this reason, a geometry optimization without symmetry constraints (unable to distinguish the two states) should take into account also this difficulty.

We have therefore decided to perform the geometry optimization for this state with the C_{2h} symmetry constraint. This reduces some of the possible problems, like the interaction of the state under study with the low-lying $2\,^1A_g^-$ state, and it remains a reasonable choice if one considers that in the experimental spectrum the vibronic progression is not very pronounced. Moreover, as discussed in Ref. [25], the knowledge of the optimized planar

Table 10 Bond lengths (Å) and angles (degrees) for the $1\,^1B_u^+$ state of *trans*-hexatriene computed at the CASSCF(2,2) and RASSCF (see text) level

Parameter	$1\,^1B_u^+$	
	CASSCF(2,2)	RASSCF
C_1–C_2	1.384	1.396
C_2–C_3	1.392	1.405
C_3–C_3'	1.417	1.431
C_1–H_1	1.073	1.077
C_1–H_2	1.075	1.080
C_2–H_3	1.079	1.079
C_3–H_4	1.076	1.079
$\theta(C_1C_2C_3)$	127.19	126.29
$\theta(C_2C_3C_{3'})$	122.09	122.72
$\theta(H_1C_1H_2)$	118.06	118.30
$\theta(C_3C_2H_3)$	116.44	116.60

structure allows to identify the energetic effects of significant changes in the bond lengths in this excited state. The geometry optimization has been performed at to different levels. The simplest is CAS (2,2) (only the HOMO and LUMO orbitals are active): With this active space, only one state of ^1B_u symmetry can be described and the problem of state mixing is therefore avoided by construction. As an alternative, we have considered a small modification of the strategy proposed in Ref. [25]: The $1\,^1B_u^+$ state is described with a RASSCF wave function, in which RAS 2 is made up of 6 π orbitals, RAS1 contains 12 σ orbitals and RAS3 12 σ^* orbitals. As indicated in Ref. [25] only one hole and one electron have been allowed in RAS1 and RAS3, respectively. With this strategy the wave function accounts for the dynamics σ polarization [25–27, 87], an important effect which is particularly relevant for the ionic states, as $1\,^1B_u^+$. The introduction of this effect stabilizes the $1\,^1B_u^+$ state more than the close-lying (neutral) $2\,^1B_u^-$ state, making $1\,^1B_u^+$ the lowest state in this symmetry and thus allowing to perform the geometry optimization. The geometrical parameters are listed in Table 10. The two strategies gives similar geometries, which correspond to a structure where the C_1-C_2 and C_2-C_3 bond lengths are intermediate between the typical single and double bond lengths, while the C_3-$C_{3'}$ bond is almost a single bond. Using these optimized geometries one can consider that the computed values are upper bound for the $1\,^1B_u^+ \leftarrow 1\,^1A_g^-$ adiabatic transition energies. Moreover, it has not been possible to obtain the $2\,^1B_u^-$ vibrational frequencies and thus to evaluate the ZPVE correction (supposed to reduce the excitation energy).

The main geometrical values obtained with the cc-pVTZ basis set and a full description of the equilibrium geometry (in cartesian coordinates) of the $1\,^1B_u^+$ state,

Table 11 Adiabatic excitation energies (eV) for the $1\,^1B_u^+ \leftarrow 1\,^1A_g^-$ transition of *trans*-hexatriene calculated with the C_{2h} CASSCF (2,2) and RASSCF (see text) optimized geometry for the $1\,^1B_u^+$ state

	$1\,^1B_u^+ \leftarrow 1\,^1A_g^-$			
	CASSCF	MS-CASPT2	QD-SC2	QD-PC2
CAS (2,2) geom.				
CAS (6,6)	7.008	4.972(4.573)	4.517	4.349
CAS (6,8)	6.478	5.164(4.897)	4.994	4.934
CAS (6,10)	6.392	5.135(4.901)	5.156	5.064
CAS (6,12)	6.246	5.066(4.850)	5.246	5.111
CAS (6,14)	6.121	5.088(4.886)	5.320	5.186
RASSCF geom.				
CAS (6,6)	7.009	4.971(4.569)	4.482	4.318
CAS (6,8)	6.487	5.181(4.934)	4.967	4.905
CAS (6,10)	6.380	5.160(4.942)	5.119	5.039
CAS (6,12)	6.240	5.126(4.933)	5.201	5.090
CAS (6,14)	6.117	5.177(5.002)	5.265	5.165

CASPT2 values are computed with the IPEA = 0.25 zeroth-order Hamiltonian. Values in brackets refer to CASPT2 performed with IPEA = 0

are reported in Tables S.16 and S.17 of Suppl. Inform., respectively.

The adiabatic excitations (reported in Table 11) are lower in energy than the vertical excitations by 0.3–0.4 eV and this seems to confirm the general assumption that the two values are rather close to each other [91]. This result

Table 12 Vertical emission energies (eV) for the $1\,^1A_g^- \leftarrow 1\,^1B_u^+$ transition of *trans*-hexatriene computed with the C_{2h} optimized geometry for the $1\,^1B_u^+$ state

	$1\,^1A_g^- \leftarrow 1\,^1B_u^+$			
	CASSCF	MS-CASPT2	QD-SC2	QD-PC2
CAS (2,2) geometry				
CAS (6,6)	6.717	4.678(4.715)	4.238	4.073
CAS (6,8)	6.171	4.911(4.675)	4.653	4.653
CAS (6,10)	6.083	4.887(4.678)	4.863	4.772
CAS (6,12)	5.964	4.812(4.616)	4.918	4.812
CAS (6,14)	5.819	4.841(4.661)	5.048	4.923
RASSCF geometry				
CAS (6,6)	6.695	4.683(4.352)	4.172	4.009
CAS (6,8)	6.153	4.898(4.686)	4.655	4.595
CAS (6,10)	6.042	4.822(4.694)	4.799	4.720
CAS (6,12)	5.927	4.842(4.675)	4.856	4.764
CAS (6,14)	5.784	4.903(4.753)	4.967	4.876

CASPT2 values are computed with the IPEA = 0.25 zeroth-order Hamiltonian. Values in brackets refer to CASPT2 performed with IPEA = 0

is in reasonable agreement with the previous finding of a relaxation energy of 0.55 eV [25, 87]. Of course, it is not easy to compare the results with the experimental value of 4.93 eV [20, 84, 85], because there are crucial uncertainties about the quality of the optimized geometry and about the lack of information from the frequency analysis. Nonetheless, assuming a negative ZPVE correction of $-0.1/-0.2$ eV (similar to the values obtained for the $2\,^1A_g^-$ state), we can consider the NEVPT2 and the CASPT2 results for the $1\,^1B_u^+$ state satisfactory.

The vertical emissions are reported in Table 12. From these values, we can estimate a destabilization of 0.2–0.3 eV for the ground state at the $1\,^1B_u^+$ optimized geometry with respect to its equilibrium geometry.

The values computed with the cc-pVTZ basis set (see Tables S.18 and S.19 of Suppl. Inform.) show only minor variations with respect to those here discussed.

4.2 *cis*-hexatriene

The strategy reported in the previous section has been applied also to *cis*-hexatriene, performing the geometry optimization for the first two excited states. The $2\,^1A_1$ state, optimized at the CASSCF (6,6) level within the C_{2v} symmetry constraint, is characterized by two imaginary vibrational frequencies. All considerations previously reported for the PES of the $2\,^1A_g^-$ state of the *trans* isomer are still valid. Indeed, also for this isomer two minima have been identified, which are virtually degenerate and show a very low stabilization if compared to the C_{2v} optimized structure. Starting from the C_{2v} minimum, the $2\,^1A_1$ state is stabilized by an out-of-plane rotation of the terminal hydrogen atoms which at the optimal geometry are about 10-20 degrees out of the molecular plane. The rest of the molecule is, to a good approximation, still planar and differs from the ground state

Table 13 Bond lengths (Å) and angles (degrees) for the $2\,^1A_1$ state of *cis*-hexatriene

	$2\,^1A_1$	
	NEVPT	CASSCF
$C_1{-}C_2$	1.456	1.468
$C_2{-}C_3$	1.376	1.385
$C_3{-}C_3'$	1.446	1.445
$C_1{-}H_1$	1.078	1.072
$C_1{-}H_2$	1.079	1.074
$C_2{-}H_3$	1.074	1.074
$C_3{-}H_4$	1.076	1.077
$\theta(C_1C_2C_3)$	122.89	123.32
$\theta(C_2C_3C_3')$	122.89	126.86
$\theta(H_1C_1H_2)$	118.47	118.52
$\theta(C_3C_2H_3)$	119.83	119.93

Table 14 Adiabatic excitation energies (eV) for the $2\,^1A_1 \leftarrow 1\,^1A_1$ transition of *cis*-hexatriene computed with the C_{2v} CASSCF (6,6) optimized geometry for the $2\,^1A_1$ state with Δ (ZPVE)$= -0.225$ eV included

Parameter	$2\,^1A_1 \leftarrow 1\,^1A_1$			
	CASSCF	MS-CASPT2	QD-SC2	QD-PC2
	Δ (ZPVE)$= -0.225$			
CAS (6,6)	4.147	4.171(3.712)	4.374	4.353
CAS (6,8)	4.141	4.150(3.788)	4.278	4.255
CAS (6,10)	4.125	4.147(3.784)	4.293	4.272
CAS (6,12)	4.142	4.136(3.848)	4.355	4.311
CAS (6,14)	4.147	4.143(3.911)	4.260	4.230

CASPT2 values are computed with the IPEA = 0.25 zeroth-order Hamiltonian. Values in brackets refer to CASPT2 performed with IPEA = 0

structure merely by the modification of the bond lengths within the carbon skeleton. Moreover, the exact topology of the PES of this state in the region of the energy minimum is expected to depend on the computational parameters, such as the basis set, for example. The molecule in the $2\,^1A_1$ state is assumed to be very flexible [68].

Given that the situation closely resembles that of the $2\,^1A_g^-$ state of *trans*-hexatriene for which we have verified that the adiabatic excitation energies do not depend on the use of the exact or of the C_{2h} optimal geometry and that the values obtained with the NEVPT2 geometry are very close to those computed at the CASSCF geometry, we have chosen to discuss here the adiabatic excitations and the vertical emissions using for the $2\,^1A_1$ state the C_{2v} CASSCF optimized geometry (the parameters are in Table 13; more details concerning the comparison with the cc-pVTZ basis set and the cartesian coordinates of the equilibrium geometries are reported in Tables S.20 and S.21 of Suppl. Inform.).

The results are reported in Tables 14 (adiabatic excitation energies) and 15 (vertical emission energies). It is worth

Table 15 Vertical emission energies (eV) for the $1\,^1A_1 \leftarrow 2\,^1A_1$ transition of *cis*-hexatriene computed with the C_{2v} optimized geometry for the $2\,^1A_1$ state

	$1\,^1A_1 \leftarrow 2\,^1A_1$			
	CASSCF	MS-CASPT2	QD-SC2	QD-PC2
CAS (6,6)	3.494	3.560(3.192)	3.706	3.689
CAS (6,8)	3.491	3.531(3.244)	3.680	3.663
CAS (6,10)	3.454	3.534(3.238)	3.652	3.636
CAS (6,12)	3.473	3.540(3.209)	3.649	3.633
CAS (6,14)	3.458	3.558(3.378)	3.601	3.588

CASPT2 values are computed with the IPEA = 0.25 zeroth-order Hamiltonian. Values in brackets refer to CASPT2 performed with IPEA = 0

Table 16 Bond lengths (Å) and angles (degrees) for the $1\,^1B_2$ state of *cis*-hexatriene computed at the CASSCF(2,2) and RASSCF (see text) level

Parameter	$1\,^1B_2$	
	CASSCF(2,2)	RASSCF
C_1–C_2	1.384	1.394
C_2–C_3	1.393	1.405
C_3–C_3'	1.420	1.437
C_1–H_1	1.075	1.078
C_1–H_2	1.075	1.080
C_2–H_3	1.076	1.078
C_3–H_4	1.076	1.079
$\theta(C_1C_2C_3)$	126.29	125.25
$\theta(C_2C_3C_3')$	125.93	125.83
$\theta(H_1C_1H_2)$	118.02	118.17
$\theta(C_3C_2H_3)$	118.03	117.86

highlighting that the 0–0 adiabatic excitation energy has been directly measured (4.26 eV [67–69]) and it is, therefore, one of the experimental values known without any ambiguity. The computed values are in very good agreement with this value (4.1 eV for CASPT2 and 4.2–4.3 eV for NEVPT2) and this agreement is confirmed also for the values computed with the cc-pVTZ basis set which show a small increase of the computed transition energies (of the order of 0.1 eV, see Tables S.22 and S.23 of Suppl. Inform.).

As found for *trans*-hexatriene, one can note a marked decrease of the energy of the $2\,^1A_1$ state moving from the equilibrium geometry of the ground state to that of the $2\,^1A_1$

Table 17 Adiabatic excitation energies (eV) for the $1\,^1B_2 \leftarrow 1\,^1A_1$ transition of *cis*-hexatriene computed with the C_{2v} CASSCF (2,2) and RASSCF optimized geometries for the $1\,^1B_2$ state

	$1\,^1B_2 \leftarrow 1\,^1A_1$			
	CASSCF	MS-CASPT2	QD-SC2	QD-PC2
CAS (2,2) geometry				
CAS (6,6)	6.964	4.964(4.575)	4.491	4.331
CAS (6,8)	6.428	5.162(4.884)	4.679	4.816
CAS (6,10)	6.266	5.113(4.879)	5.055	4.967
CAS (6,12)	6.111	5.054(4.818)	5.241	5.093
CAS (6,14)	6.047	4.920(4.669)	5.339	5.138
RASSCF geometry				
CAS (6,6)	6.995	4.950(4.554)	4.459	4.299
CAS (6,8)	6.450	5.170(4.907)	4.852	4.792
CAS (6,10)	6.285	5.126(4.911)	5.025	4.947
CAS (6,12)	6.138	5.145(4.956)	5.189	5.074
CAS (6,14)	6.118	5.104(4.905)	5.238	5.120

CASPT2 values are computed with the IPEA = 0.25 zeroth-order Hamiltonian. Values in brackets refer to a CASPT2 calculation with the IPEA = 0 zeroth-order Hamiltonian

Table 18 Vertical emission energies (eV) for the $1\,^1A_1 \leftarrow 1\,^1B_2$ transition of *cis*-hexatriene computed with the C_{2v} optimized geometry for the $1\,^1B_2$ state

	$1\,^1A_1 \leftarrow 1\,^1B_2$			
	CASSCF	MS-CASPT2	QD-SC2	QD-PC2
CAS (2,2) geometry				
CAS (6,6)	6.704	4.739(4.382)	4.244	4.086
CAS (6,8)	6.164	4.931(4.684)	4.688	4.625
CAS (6,10)	6.009	4.898(4.689)	4.834	4.747
CAS (6,12)	5.834	4.840(4.625)	4.984	4.845
CAS (6,14)	5.778	4.718(4.486)	5.086	4.896
RASSCF geometry				
CAS (6,6)	6.664	4.662(4.306)	4.148	3.990
CAS (6,8)	6.133	4.872(4.646)	4.607	4.548
CAS (6,10)	5.963	4.851(4.667)	4.746	4.668
CAS (6,12)	5.815	4.872(4.709)	4.839	4.746
CAS (6,14)	5.779	3.830(4.655)	4.929	4.822

CASPT2 values are computed with the IPEA = 0.25 zeroth-order Hamiltonian. Values in brackets refer to CASPT2 performed with IPEA = 0

state (1.2–1.3 eV, compare the value in Table 14 without the Δ (ZPVE) term with those in Table 5) and a marked increase of the ground state energy along the same nuclear displacement (0.8–0.9 eV, compare the value in Table 14 without the Δ (ZPVE) term with those in Table 15). The two variations are, however, rather different, thus questioning also for the $2\,^1A_1$ state of *cis*-hexatriene the possible use of the mirror image symmetry rule [88].

The strategy applied in Sect. 4.1 for the geometry optimization of the ionic $1\,^1B_u^+$ state of *trans*-hexatriene (optimization at the CASSCF (2,2) and RASSCF levels) has been applied also for the $1\,^1B_2$ state of *cis*-hexatriene without any problem in the convergence procedure. The main geometrical parameters are reported in Table 16 (see Tables S.24 and S.25 of Suppl. Inform. for the comparison with the cc-pVTZ basis set and the cartesian coordinates of the equilibrium geometries) and one can note that the central C–C bond is almost a single bond (in particular at the RASSCF level), while the other C–C bonds are intermediate between a single and a double bond. Also in this case, we have not been able to compute the vibrational frequencies at the optimal C_{2v} geometry.

The $1\,^1B_2 \leftarrow 1\,^1A_1$ adiabatic excitation energies are reported in Table 17, while the $1\,^1A_1 \leftarrow 1\,^1B_2$ vertical emission energies are in Table 18. The dependence of the transition energies on the computational details (dimension of the active space, inclusion of the dynamic correlation, geometry) strictly follows what reported in Sect. 4.1 for the $1\,^1B_u^+$ state of *trans*-hexatriene (see the comments on the values in Tables 11 and 12).

For the $1\,^1B_2 \leftarrow 1\,^1A_1$ adiabatic excitation energy computed with the largest active space at the CASSCF (2,2) geometry, one notes a slightly worse agreement of the various MRPT2: The SC-NEVPT2 value differs from the PC-NEVPT2 one by 0.2 eV and the same is true comparing PC-NEVPT2 and CASPT2(IPEA = 0.25). This behavior anomalous in this study. Our best estimations for this quantity is 5.1–5.2 eV from the NEVPT2 results and 5.1 eV for CASPT2(IPEA = 0.25). These values are in good agreement with the experimental value, 4.92 eV [83, 92], if one considers that the zero point vibrational energy correction has not been taken into account and that this quantity is expected to be negative, in the range −0.1/−0.2 eV. The experimental value corresponds to the first and more intense peak in the experimental spectrum. For this reason, this value has been also indicated as the experimental vertical excitation energy. Our study reveals that the vertical and adiabatic $1\,^1B_2 \leftarrow 1\,^1A_1$ are actually rather close, but they differ by at least by $\simeq$ 0.3–0.4 eV (NEVPT2) and $\simeq$ 0.2–0.3 eV (CASPT2).

Finally, for the vertical $1\,^1A_1 \leftarrow 1\,^1B_2$ emission energy, the best estimation is 4.8–4.9 eV (NEVPT2) and 4.9 eV (CASPT2(IPEA = 0.25)), indicating that the ground state is destabilized by 0.2–0.3 eV passing from its equilibrium geometry to the $1\,^1B_2$ equilibrium geometry (constrained to belong the C_{2v} symmetry).

The relatively small energy change of ground and $1\,^1B_2$ states when moving from the ground state equilibrium geometry to that of the $1\,^1B_2$ state confirms the hypothesis (deduced from the vibrational progression in the experimental spectrum) that the two geometries are rather close to each other.

Also, for *cis*-hexatriene the results obtained with the cc-pVTZ confirm the conclusions here reported, in general with the excitation energies only slightly higher (see Tables S.26 and S.27 of Suppl. Inform.).

Table 19 *Trans*-hexatriene: comparison of the transition energies (eV) obtained in this work (best estimates) with those obtained in previous theoretical works and with the experimental value

Method	vert. $2\,^1A_g^- \leftarrow 1\,^1A_g^-$	vert. $1\,^1B_u^+ \leftarrow 1\,^1A_g^-$	adiab. $2\,^1A_g^- \leftarrow 1\,^1A_g^-$	adiab. $1\,^1B_u^+ \leftarrow 1\,^1A_g^-$
SC-NEVPT2	5.55–5.59	5.62–5.65	4.34	5.26–5.32
PC-NEVPT2	5.55–5.59	5.48–5.51	4.34	5.16–5.19
CASPT2(IPEA = 0.25)	5.42–5.46	5.36–5.39	4.19–4.21	5.09–5.18
CASPT2(IPEA = 0.0)	5.20–5.24	5.17–5.19	3.95–3.98	4.89–5.00
CC3 [59]	5.72	5.58		
CCSDR(3)/cc-pVDZ]+5 [91]	6.06	5.40		
CASPT2	5.19 [65] 5.21 [70] 5.42 [59] 5.52 [76]	5.04 [86] 5.01 [65] 5.08 [70] 5.31 [59] 5.34 [76]		
MSCAS(10,10)PT2 [78]	5.45	5.19		
DFT-SSMRPT(6,6)/cc-pVQZ [79]	4.99	4.78		
RSPT2(8,8) [93]	5.01	5.12		4.32
NEVPT2 [76]	5.5–5.6	4.84–4.94		
SC-NEVPT2 [70]	5.60	5.35		
RASSCF(32,13+6+19) [25]			4.46	
CI [87]			4.52	
Experimental	5.21 [16]	4.93 [83–85] 5.08 [16]	$\geq$ 4.22 [69]	4.93 [83–85]

Table 20 *Cis*-hexatriene: comparison of the transition energies (eV) obtained in this work (best estimates) with those obtained in previous theoretical works and with the experimental value

	vert. $2\,^1A_1 \leftarrow 1\,^1A_1$	vert. $1\,^1B_2 \leftarrow 1\,^1A_1$	adiab. $2\,^1A_1 \leftarrow 1\,^1A_1$	adiab. $1\,^1B_2 \leftarrow 1\,^1A_1$
SC-NEVPT2	5.47–5.52	5.60–5.63	4.26	5.24–5.34
PC-NEVPT2	5.43–5.48	5.46–5.49	4.23	5.12–5.14
CASPT2(IPEA = 0.25)	5.35–5.40	5.41–5.44	4.14	5.10
CASPT2(IPEA = 0.0)	5.13–5.17	5.15–5.20	3.91	4.90
RSPT2(10,10) [93]	5.00	5.30	4.29	4.94
Experimental		4.92 [83, 92]	4.26 [67–69]	4.92 [83, 92]

5 Interpretation of the experimental data and comparison with previous theoretical works

The transition energies obtained in the present study, together with the values from a selection of previously published theoretical works and from experimental studies, are reported in Table 19 for *trans*-hexatriene and Table 20 for *cis*-hexatriene.

In order to discuss these results, it is worth recalling that to the aim of the present work, there are only a few experimental values which are clearly defined, all concern adiabatic (0–0) transitions. In details, they are: the adiabatic $1\,^1B_u^+ \leftarrow 1\,^1A_g^-$ transition of *trans*-hexatriene (4.93 eV [83–85]), the adiabatic $1\,^1B_2 \leftarrow 1\,^1A_1$ transition of *cis*-hexatriene (4.92 [83, 92]), and the adiabatic $2\,^1A_g^- \leftarrow 1\,^1A_g^-$ transition of *trans*-hexatriene (4.26 eV [67–69]). Moreover, the adiabatic $2\,^1A_1 \leftarrow 1\,^1A_1$ transition of *cis*-hexatriene has a clear experimental indication (≥ 4.22 eV [69]).

From the theoretical point of view, the adiabatic transitions to the ionic states ($1\,^1B_u^+$ and $1\,^1B_2$ for *trans*-hexatriene and *cis*-hexatriene, respectively) are difficult to reproduce at a very high level, because the full geometry optimization for these states is a very difficult task. Moreover, the two states involved in the transition have a different nature (ionic for the excited state, neutral for the ground state), and this implies that the dynamic electron correlation is also different, both quantitatively (larger in the ionic state) and qualitatively (the dynamic σ polarization is more important in the ionic state).

On the contrary, the adiabatic transitions to the neutral states ($2\,^1A_g^-$ and $2\,^1A_1$ for *trans*-hexatriene and *cis*-hexatriene, respectively) can be computed at a high level, given that the equilibrium geometry for these states can be obtained and that the two states involved in the transition have the same nature (neutral) and also very similar dynamic electron correlation energies. These adiabatic transitions are very well reproduced by our approach with values which remain relatively stable by changing the computational details.

This is a pivotal achievement of the present work: For an experimental value which is known without ambiguity (it is directly extracted from the experimental spectrum) the approach here used (atomic basis set, geometry optimization, strategy for the inclusion of the static and of the dynamic electron correlation) gives results very close to the experimental finding.

For the adiabatic transition to the ionic bright states ($1\,^1B_u^+$ and $1\,^1B_2$ for *trans*-hexatriene and *cis*-hexatriene, respectively), the results here obtained are also in reasonable agreement with the experimental values, if one takes into account that the true equilibrium geometry of these states has not been found and that the lack of the vibrational frequencies prevent us from estimating the zero vibrational energy difference between the two states.

The good agreement for these values allows to look with more attention at the vertical excitation energies, where a partial disagreement between our results and the "experimental" values seems to emerge. The analysis of this partial disagreement must take into account the fact that for both isomers of hexatriene the vertical excitation energies are not directly observable in the experimental spectra, but are obtained from the data extracted from the experimental spectra by means of some educated guesses.

6 Conclusions

In this work, the main aspects of the spectroscopy of hexatriene have been considered within a multireference perturbation theory (MRPT) approach. As a first aspect, one can consider the comparison of two different MRPT2 theories, CASPT2 (IPEA = 0.25) and NEVPT2. These two different MRPT2 approaches show in general a very good agreement, in particular with large active space (as already observed, see Refs. [60, 94] for a few examples). For the smallest active spaces, the excitation energies (both vertical and adiabatic) are very close for the $2\,^1A_g^-$ state of *trans*-hexatriene and for the $2\,^1A_1$ state of *cis*-hexatriene, while for the $1\,^1B_u^+$ state of *trans*-hexatriene and for the $1\,^1B_2$ state of *cis*-hexatriene they give quite different transition energies. The agreement is recovered also for these states by enlarging the active space. On the contrary, CASPT2 (IPEA = 0.0) gives constantly lower values (of both CASPT2 (IPEA = 0.25) and NEVPT2) for the transition energies. In all cases, the vertical excitation energies do not show a marked dependence on the level of theory (NEVPT2 or CASSCF) used to optimize the ground state geometry. The good agreement of the CASPT2 (IPEA = 0.25) and NEVPT2 approaches with the experimental data (the adiabatic transitions) shows that the modification proposed in CASPT2 with the introduction of the IPEA shift [46] is effective (at least for the systems here considered) and gives better results than the original version.

A second aspect considered is the geometry optimization of the covalent excited states ($2\,^1A_g^-$ for the *trans* isomer, $2\,^1A_1$ for the *cis* isomer). In these states, a clear inversion of single and double bonds occurs. Even if the frequency analysis indicates an equilibrium geometry where the symmetry of the ground state is lost (the molecule is no longer planar), the rotations of the terminal C–CH$_2$ groups is essentially barrierless and the energy of the state does not vary appreciably. So, there are no practical reasons to choose a fully optimized geometry and it is possible to consider for this state a geometry with the same symmetry as the ground state.

The most challenging issue has been the geometry optimization of the ionic excited states, as described in Sect. 4.1. The solution adopted is based on the assumption of the preservation of the symmetry of the ground state equilibrium geometry. This choice is partially justified by the vibrational progression of the experimental spectrum. The key question is how to obtain a balanced treatment of the two states of B_u and B_1 symmetry for *trans-* and *cis-*hexatriene, respectively, and to avoid the root flipping problem during the optimization process. We have used two different strategies (one of which proposed in Ref. [25]) to perform this task and the final geometries are rather close to each other, as happens also for the excitation energies. With these strategies an upper bound for the adiabatic excitation energies is obtained. The results do not markedly differ from the vertical excitation energies and can be considered satisfactory, especially if one considers that the ZPVE correction is not included.

The vertical excitation energies reported in this work for both isomers, while confirming that the first two excited states of hexatriene are in general virtually degenerate in the Franck–Condon region, are higher than the reference previously published values. In this case, what is reported as "experimental values" are actually educated guesses from the experimental data using some assumption. The good agreement with the experimental values found for the adiabatic transition energies and the presence of not fully grounded assumptions in the definition of the "experimental values" for the vertical excitation energies makes reliable the values here computed.

Declarations

References

1. Pariser R (1956) J Chem Phys 24:250. https://doi.org/10.1063/1.1742461
2. Nakayama K, Nakano H, Hirao K (1998) Int J Quantum Chem 66:157. https://onlinelibrary.wiley.com/doi/pdf/10.1002/%28SICI%291097-461X%281998%2966%3A2%3C157%3A%3AAID-QUA7%3E3.0.CO%3B2-U
3. Mikhailov IA, Tafur S, Masunov AE (2008) Phys Rev A 77:012510
4. Angeli C, Guihéry N, Malrieu JP (2023) In: Reference module in chemistry, molecular sciences and chemical engineering, Elsevier
5. Szabo A, Langlet J, Malrieu J-P (1976) Chem Phys 13:173
6. Said M, Maynau D, Malrieu JP (1984) J Am Chem Soc 106:580. https://doi.org/10.1021/ja00315a020
7. Robert V, Malrieu J-P (2004) J Chem Phys 120:8853
8. Angeli C, Malrieu J-P (2008) J Phys Chem A 112:11481. https://doi.org/10.1021/jp805870r
9. Tenti L, Giner E, Malrieu J-P, Angeli C (2017) Comput Theor Chem 1116:102 (**understanding Chemistry and Biochemistry Using Computational Valence Bond Theory**)
10. Accomasso D, Persico M, Granucci G (2019) ChemPhotoChem 3:933. https://doi.org/10.1002/cptc.201900056
11. Suaud N, Amor N, Guihéry N, Malrieu J-P (2021) Theor Chem Acc 140:117
12. Malrieu J-P, Guihéry N, Calzado CJ, Angeli C (2007) J Comput Chem 28:35. https://doi.org/10.1002/jcc.20546
13. Angeli C, Cimiraglia R, Malrieu J-P (2008) J Chem Educ 85:150. https://doi.org/10.1021/ed085p150
14. Angeli C, Cimiraglia R, Malrieu J-P (2013) Mol Phys 111:1069. https://doi.org/10.1080/00268976.2013.771803
15. Angeli C, Del Re G, Persico M (1995) Chem Phys Lett 233:102
16. Fujii T, Kamata A, Shimizu M, Adachi Y, Maeda S (1985) Chem Phys Lett 115:369
17. Angeli C, Pastore M (2011) J Chem Phys 134:184302. https://doi.org/10.1063/1.3585607
18. Zhang D, Liu C (2011) J Chem Phys 135:134117. https://doi.org/10.1063/1.3643838
19. Pariser R, Parr RG (1953) J Chem Phys 21:767. https://doi.org/10.1063/1.1699030
20. Gavin RM, Risemberg S, Rice SA (1973) J Chem Phys 58:3160. https://doi.org/10.1063/1.1679637
21. Gavin RM, Weisman C, McVey JK, Rice SA (1978) J Chem Phys 68:522. https://doi.org/10.1063/1.435761
22. Garavelli M, Celani P, Bernardi F, Robb MA, Olivucci M (1997) J Am Chem Soc 119:11487. https://doi.org/10.1021/ja971280u
23. Ci X, Myers AB (1992) J Chem Phys 96:6433. https://doi.org/10.1063/1.462608
24. Davidson ER (1996) J Phys Chem 100:6161. https://doi.org/10.1021/jp952794n
25. Boggio-Pasqua M, Bearpark MJ, Klene M, Robb MA (2004) J Chem Phys 120:7849. https://doi.org/10.1063/1.1690756
26. Angeli C (2010) Int J Quantum Chem 110:2436. https://doi.org/10.1002/qua.22597
27. Angeli C (2009) J Comput Chem 30:1319. https://doi.org/10.1002/jcc.21155
28. Angeli C, Improta R, Santoro F (2009). J Chem Phys. https://doi.org/10.1063/1.3131263174307
29. Cimiraglia R, Persico M (1987) J Comput Chem 8:39. https://doi.org/10.1002/jcc.540080105
30. Angeli C, Cimiraglia R, Persico M, Toniolo A (1997) Theor Chem Acc 98:57
31. Angeli C, Persico M (1997) Theor Chem Acc 98:117

32. Cimiraglia R, Persico M (1979) Mol Phys 38:1707. https://doi.org/10.1080/00268977900102781
33. Cimiraglia R, Malrieu JP, Persico M, Spiegelmann F (1985) J Phys B Atom Mol Phys 18:3073
34. Cattaneo P, Persico M (1997) Chem Phys 214:49
35. Cattaneo P, Persico M (1999) Phys Chem Chem Phys 1:4739
36. Granucci G, Persico M, Toniolo A (2001) J Chem Phys 114:10608
37. Toniolo A, Persico M (2001) J Comput Chem 22:968. https://doi.org/10.1002/jcc.1057
38. Barbatti M, Granucci G, Persico M, Lischka H (2005) Chem Phys Lett 401:276
39. Plasser F, Granucci G, Pittner J, Barbatti M, Persico M, Lischka H (2012). J Chem Phys. https://doi.org/10.1063/1.473896022A514
40. Persico M, Granucci G (2014) Theor Chem Acc 133:1–28. https://doi.org/10.1007/s00214-014-1526-1
41. Barbatti M, Ruckenbauer M, Plasser F, Pittner J, Granucci G, Persico M, Lischka H (2014) WIREs Comput Mol Sci 4:26. https://doi.org/10.1002/wcms.1158
42. Cantatore V, Granucci G, Persico M (2014) Comput Theor Chem 1040–1041:126 (**excited states: From isolated molecules to complex environments**)
43. Dunning J, Thom H (1989) J Chem Phys 90:1007
44. Andersson K, Malmqvist P-A, Roos BO (1992) J Chem Phys 96:1218. https://doi.org/10.1063/1.462209
45. Roos BO, Andersson K (1995) Chem Phys Lett 245:215
46. Ghigo G, Roos BO, Malmqvist P-A (2004) Chem Phys Lett 396:142
47. Forsberg N, Malmqvist P-A (1997) Chem Phys Lett 274:196
48. Aquilante F, De Vico L, Nicolas F, Ghigo G, Malmqvist P-Å, Neogrády P, Pedersen TB, Pitoňák M, Reiher M, Roos BO, Serrano-Andrés L, Urban M, Veryazov V, Lindh R (2010) J Comput Chem 31:224. https://doi.org/10.1002/jcc.21318
49. Galván IFdez, Vacher M, Alavi A, Angeli C, Aquilante F, Autschbach J, Bao JJ, Bokarev SI, Bogdanov NA, Carlson RK, Chibotaru LF, Creutzberg J, Dattani N, Delcey MG, Dong SS, Dreuw A, Freitag L, Frutos LM, Gagliardi L, Gendron F, Giussani A, González L, Grell G, Guo M, Hoyer CE, Johansson M, Keller S, Knecht S, Kovačević G, Källman E, Li Manni G, Lundberg M, Ma Y, Mai S, Malhado JAP, Malmqvist PAK, Marquetand P, Mewes SA, Norell J, Olivucci M, Oppel M, Phung QM, Pierloot K, Plasser F, Reiher M, Sand AM, Schapiro I, Sharma P, Stein CJ, Sørensen LK, Truhlar DG, Ugandi M, Ungur L, Valentini A, Vancoillie S, Veryazov V, Weser O, Wesolowski TA, Widmark P-O, Wouters S, Zech A, Zobel JP, Lindh R (2019) J Chem Theory Comput 15:5925. https://doi.org/10.1021/acs.jctc.9b00532
50. Angeli C, Cimiraglia R, Evangelisti S, Leininger T, Malrieu J-P (2001) J Chem Phys 114:10252. https://doi.org/10.1063/1.1361246
51. Angeli C, Cimiraglia R, Malrieu J-P (2001) Chem Phys Lett 350:297
52. Angeli C, Cimiraglia R, Malrieu J-P (2002) J Chem Phys 117:9138. https://doi.org/10.1063/1.1515317
53. Angeli C, Pastore M, Cimiraglia R (2007) Theor Chem Acc 117:743
54. Angeli C, Borini S, Cestari M, Cimiraglia R (2004) J Chem Phys 121:4043. https://doi.org/10.1063/1.1778711
55. Neese F (2012) WIREs Comput Mol Sci 2:73. https://doi.org/10.1002/wcms.81
56. Dyall KG (1995) J Chem Phys 102:4909. https://doi.org/10.1063/1.469539
57. Finley J, KeMalmqvist P-A, Roos BO, Serrano-Andrés L (1998) Chem Phys Lett 288:299
58. Bomble YJ, Sattelmeyer KW, Stanton JF, Gauss J (2004) J Chem Phys 121:5236. https://doi.org/10.1063/1.1780159
59. Schreiber M, Silva-Junior MR, Sauer SPA, Thiel W (2008). J Chem Phys. https://doi.org/10.1063/1.2889385134110
60. Valsson O, Angeli C, Filippi C (2012) Phys Chem Chem Phys 14:11015
61. Zobel JP, Nogueira JJ, González L (2017) Chem Sci 8:1482
62. Wolanski L, Grabarek D, Andruninóv T (2018) J Comput Chem 39:1470. https://doi.org/10.1002/jcc.25217
63. Kepenekian V, Robert M, Le Guennic B (2009). J Chem Phys. https://doi.org/10.1063/1.3211020114702
64. Vela S, Fumanal M, Ribas-AriñJordi, Robert V (2016) J Comput Chem 37:947. https://doi.org/10.1002/jcc.24283
65. Serrano-Andrés L, Merchán M, Nebot-Gil I, Lindh R, Roos BO (1993) J Chem Phys 98:3151. https://doi.org/10.1063/1.465071
66. Luo Y, Aagren H, Stafstroem S (1994) J Phys Chem 98:7782. https://doi.org/10.1021/j100083a007
67. Mcdiarmid R (1999) On the electronic spectra of small linear polyenes. In: Advances in chemical physics, John Wiley Sons Ltd., Chap. 2:177–214. https://doi.org/10.1002/9780470141694.ch2
68. Buma WJ, Kohler BE, Song K (1991) J Chem Phys 94:6367. https://doi.org/10.1063/1.460315
69. Buma WJ, Kohler BE, Song K (1990) J Chem Phys 92:4622
70. Zgid D, Ghosh D, Neuscamman E, Chan GK-L (2009). J Chem Phys. https://doi.org/10.1063/1.3132922/15860237/194107_1_online.pdf
71. Rinkevicius Z, Vahtras O, Agren H (2010). J Chem Phys. https://doi.org/10.1063/1.3479401/15430885/114104_1_online.pdf
72. Mazur G, Makowski M, Wlodarczyk R, Aoki Y (2011) Int J Quantum Chem 111:819. https://doi.org/10.1002/qua.22876
73. Casanova D (2012). J Chem Phys. https://doi.org/10.1063/1.4747341/13989964/084105_1_online.pdf
74. Tassi M, Theophilou I, Thanos S (2013). J Chem Phys. https://doi.org/10.1063/1.4797466/15460198/124107_1_online.pdf
75. Yang Y, van Aggelen H, Yang W (2013) J Chem Phys 139:224105. https://doi.org/10.1063/1.4834875/13323072/224105_1_online.pdf
76. Schapiro I, Sivalingam K, Neese F (2013) J Chem Theory Comput 9:3567. https://doi.org/10.1021/ct400136y
77. Ronca E, Angeli C, Belpassi L, De Angelis F, Tarantelli F, Pastore M (2014) J Chem Theory Comput 10:4014. https://doi.org/10.1021/ct5004675
78. Komainda A, Lyskov I, Marian CM, Köppel H (2016) J Phys Chem A 120:6541. https://doi.org/10.1021/acs.jpca.6b04971
79. Manna S, Chaudhuri RK, Chattopadhyay S (2020) J Chem Phys 152:244105. https://doi.org/10.1063/5.0007198/13893571/244105_1_online.pdf
80. Park W, Shen J, Lee S, Piecuch P, Filatov M, Choi CH (2021) J Phys Chem Lett 12:9720. https://doi.org/10.1021/acs.jpclett.1c02707
81. Fatková K, Cajzl R, Burda JV (2023) J Comput Chem 44:777. https://doi.org/10.1002/jcc.27040
82. Gozem S, Huntress M, Schapiro I, Lindh R, Granovsky AA, Angeli C, Olivucci M (2012) J Chem Theory Comput 8:4069. https://doi.org/10.1021/ct3003139
83. Minnaard NG, Havinga E (1973) Recueil des Travaux Chimiques des Pays-Bas 92:1179. https://doi.org/10.1002/recl.19730921102
84. Leopold DG, Pendley RD, Roebber JL, Hemley RJ, Vaida V (1984) J Chem Phys 81:4218. https://doi.org/10.1063/1.447453
85. Myers AB, Pranata KS (1989) J Phys Chem 93:5079. https://doi.org/10.1021/j100350a015
86. Serrano-Andrés L, Roos BO, Merchán M (1994) Theoretica Chimica Acta 87:387
87. Cave RJ, Davidson ER (1988) Chem Phys Lett 148:190
88. Christensen RL, Galinato MGI, Chu EF, Howard JN, Broene RD, Frank HA (2008) J Phys Chem A 112:12629. https://doi.org/10.1021/jp8060202
89. Lasaga AC, Aerni RJ, Karplus M (1980) J Chem Phys 73:5230. https://doi.org/10.1063/1.439951
90. Catalán J, de Paz JLG (2006) J Chem Phys 124:034306. https://doi.org/10.1063/1.2158992

91. Cronstrand P, Christiansen O, Norman P, Ågren H (2001) Phys Chem Chem Phys 3:2567
92. Sabljic A, McDiarmid R (1985) J Chem Phys 82:2559
93. Komainda A, Zech A, Köppel H (2015) J Mol Spectrosc 311:25 (**theory and Spectroscopy**)
94. Sarkar R, Loos P-F, Boggio-Pasqua M, Jacquemin D (2022) J Chem Theory Comput 18:2418. https://doi.org/10.1021/acs.jctc.1c01197